(Received 5 June 2024, Accepted 10 July 2024, Scheduled 16 July 2024)

Design of 5G Multi-Frequency Antenna Based on Multi-Objective Sequential Domain Patching

Wenjian Zhu[1], Jiayi Chen[1], Panshi Hu[2], Zhi Song[2], and Yanbing Xue[1,*]

[1]*School of Automation and Electrical Engineering, Dalian Jiaotong University, China*
[2]*School of Computer and Communication Engineering, Dalian Jiaotong University*
Applied Basic Research Project of Liaoning Science and Technology Department, Dalian 116028, China

ABSTRACT: This paper introduces a 5G multi-frequency antenna design method based on multi-objective sequential domain patching. By etching helical metamaterials on radiation patches and loading asymmetric electric-inductive-capacitive metamaterials on the transmission line side, the antenna structure is designed and optimized using electromagnetic simulation software, HFSS, and MATLAB. The resulting multi-frequency antenna operates across multiple frequency bands: n1, n41, 3.5G, and 4.9G. To ensure antenna performance and radiation efficiency, the antenna multi-frequency bands are precisely controlled. The experimental results show that the error between each operating frequency band and target frequency bands of the antenna is within 7.2%. Compared with conventional antenna design methods, the use of metamaterials and intelligent algorithms to optimize the structural parameters and loading positions of metamaterials can improve antenna performance while shortening the design cycle. Overall, this research offers novel insights into the design of 5G high-performance antennas.

1. INTRODUCTION

With advancements in information technology, 5G wireless communication systems have been widely applied in various fields. As a key component in information transmission, microstrip antennas have attracted considerable attention because of their small size, low cost, and ability to conveniently realize various polarization modes. Multi-frequency antennas offer several advantages, including reduction in the number of antennas, enhanced space utilization, and cost savings, and have thus been widely used in wireless communication, radio frequency identification, sensor networks, and multiple-input multiple-output systems [1].

Metamaterials are manufactured composite materials with unique physical properties. Many scholars have successfully integrated metamaterial structures into antenna designs and achieved promising results [2–8].

For example, split ring resonators (SRRs) have been loaded on both sides of a transmission line to realize three-band antennas operating at 2.7 GHz, 4.3 GHz, and 4.7 GHz. Additionally, two SRRs of different sizes have been loaded on one side of the antenna transmission line to derive two new operating bands [9]. In another study [10], the high-frequency band of an antenna was realized by introducing a microstrip line-excited circular slit, and the low-frequency band was achieved by improving the SRR ring. Moreover, eight identical open resonant rings have been arranged by rotation, and a central symmetric structure has been established by integrating a parasitic patch in the internal structure, characterized by multi-frequency, wide incidence angle, and insensitive polarization [11].

Notably, the design of the above-mentioned antennas is based on the parameter scanning method [9], which is computationally expensive, exhibits significant randomness, and strongly relies on design experience. To facilitate antenna design, scholars have introduced intelligent optimization algorithm into antenna structure optimization to shorten the design cycle and improve the antenna performance [12–15]. For example, certain researchers [16] proposed a multi-objective sequential domain patching (MSDP) approach combined with spatial mapping technology to optimize the structural parameters of an ultra-wideband (UWB) monopole antenna. The optimization time for the antenna was 67.7 h, less than that achieved using the non-dominated sorting genetic algorithm-II (183.3 h). Other researchers leveraged [17] the differential evolution and naked mole-rat algorithms to design a three-band antenna using a hybrid optimization method. After optimizing the structural parameters, the peak gain was 3.55 dBi, with an excellent average gain of 2.5 dBi.

Although intelligent optimization algorithms have been applied in antenna design, the optimization process has been limited to the structural parameters of the antenna. Because the loading position does not considerably influence the resonance characteristics, its optimization has not been extensively explored in conventional antenna design. However, in scenarios involving stringent antenna requirements and complex metamaterials, the antenna performance can be significantly improved by optimizing the loading position.

Thus, in this study, a four-band antenna is designed using wideband techniques, i.e., by increasing the notch and resonance. First, based on the electromagnetic theory of metamaterials, a spiral metamaterial resonant groove is designed, and

* Corresponding author: Yanbing Xue (dlxyb@djtu.edu.cn).

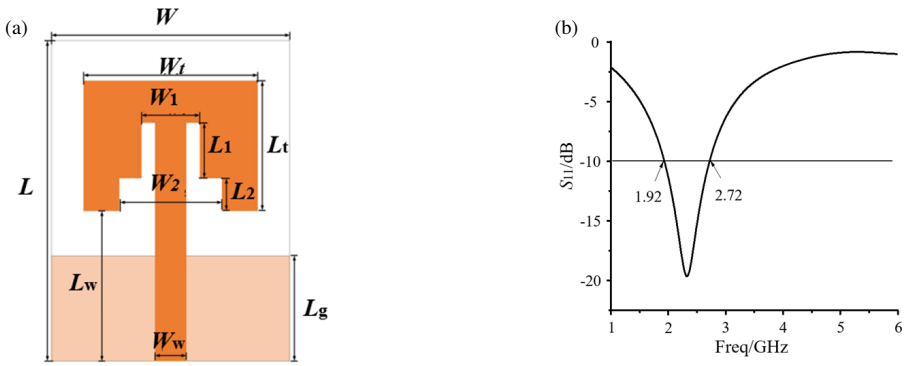

FIGURE 1. (a) Initial structure of antenna. (b) S_{11} parameter antenna.

the tail end of the C-ring is folded. The inductance is extended to miniaturize the antenna. Two low-frequency bands of the antenna are generated through the notch action of the resonant slot. Based on these aspects, the traditional electric-inductive-capacitive (ELC) resonator is improved, and an asymmetric ELC resonator is designed and loaded to the transmission line side. An antenna with two high-frequency bands is realized using the single resonant structure.

During the design phase, the MSDP algorithm and parameter scanning method are used to optimize the multi-frequency antenna. The initial structural parameters of the antenna and metamaterial, satisfying the requirements of the working frequency band, are obtained using the S-parameter scanning method. Next, the structural parameters and loading position parameters of the two metamaterials are considered the optimization variables, and the MSDP algorithm is used to optimize the structure and loading position of the metamaterials based on the S-parameter and radiation efficiency, thereby enhancing the design efficiency and antenna performance.

2. ANTENNA STRUCTURE

In general, 5G multi-frequency antennas operate within the following frequency bands: n1: 1.92–2.17 GHz, n41: 2.515–2.675 GHz, 3.5G: 3.4–3.6 GHz, and 4.9G: 4.8–5.0 GHz. First, the dual-band antenna is realized by etching a C-type spiral groove, and the four-band antenna is then established by loading the asymmetric ELC resonator.

2.1. Initial Structure

Figure 1(a) illustrates the structure of the wideband antenna with operating frequency bands n1 and n41. The broadband antenna is printed on an FR4 dielectric substrate sized 26 mm × 32 mm × 1.6 mm (Dielectric loss tan $\delta = 0.02$, dielectric constant $\varepsilon_r = 4.4$). Considering a typical rectangular patch antenna, two rectangles of different sizes are cut out in the middle of its rectangular radiation patch. The initial wideband antenna is simulated and optimized using the parameter scanning method, and the parameters of the antenna are determined as follows (unit: mm): $W = 26$, $L = 32$, $L_g = 10.5$, $L_t = 13$, $L_1 = 5.57$, $L_2 = 3.29$, $L_w = 15$, $W_t = 19$, $W_1 = 6.33$, $W_2 = 11.17$, and $W_w = 3.4$. The S-parameter simulation results show that the antenna operates at a frequency of 1.92–2.72 GHz, covering n1 and n41 frequency bands, as shown in Fig. 1(b). Thus, a dual-band antenna can be constructed by etching a resonant slot.

2.2. Dual-Band Structure

2.2.1. Spiral Metamateria

To change the broadband antenna into n1 and n41 dual-band antennas, the notch metamaterial resonance frequency range of the etching is selected to be between 2.17 and 2.515 GHz. The C-ring structure is shown in Fig. 2(a). The center frequency of the C-ring notch is calculated using Equations (1)–(3) [18]:

$$f_{\text{notch}} = \frac{1}{2\pi\sqrt{L_e C}} \tag{1}$$

$$L_e = \mu_0 l \tag{2}$$

$$C = \frac{2\varepsilon_0 l_s}{\pi} \ln \frac{2l_s}{a} \tag{3}$$

where l is the total length of the three sides without openings, corresponding to the equivalent inductance of L_e, and μ_0 is the vacuum permeability. C is the equivalent capacitance of the open side length l_s of the open ring and open gap a, and ε_0 is the electric constant of the vacuum medium.

Folding the tail end of the C-ring to form a spiral can enhance the inductance and resonance characteristics. Thus, the open edge of length l_s is folded into the structure with growth degrees of j_3, j_4, and j_5, as shown in Fig. 2(b). The spiral metamaterial unit is simulated and optimized using the parameter scanning method, and the parameters are determined as follows (unit: mm): $j_1 = 19$, $j_2 = 6$, $j_3 = 3$, $j_4 = 4$, and $j_5 = 2.5$. The S-parameter simulation of the metamaterial unit shows that the notch frequency center is 2.32 GHz. Additionally, the notch frequency center calculated by inserting the metamaterial parameters into Equations (1)–(3) is 2.23 GHz, which meets the initial design requirements.

2.2.2. Structure Design Based on MSDP Algorithm

The multi-frequency antenna operates within fixed frequency bands, and it is preferable for the operating frequency of each

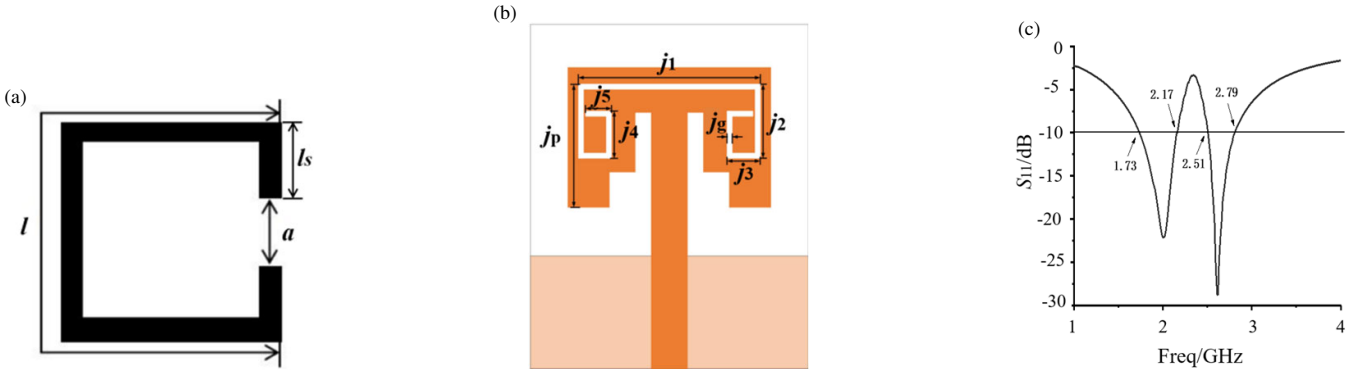

FIGURE 2. (a) C-ring structure. (b) Dual-band antenna. (c) S_{11} parameter of dual-band antenna.

frequency band to be as close as possible to the target. The structural parameters and loading position of the metamaterial must be continuously adjusted to satisfy the design requirements of the antenna. To improve the design efficiency, a co-simulation approach using HFSS and MATLAB software is used. The parameters of metamaterial structure and loading position are considered optimization variables, and the multi-objective optimization of the antenna is performed using the MSDP algorithm. The target parameters are the target frequency band and radiation efficiency.

Parameter S_{11} is optimization objective 1, and the objective function and fitness function are defined as follows:

$$\textit{fitness 1} = 0.5\textit{fitness}_{11} + 0.5\textit{fitness}_{12} \tag{4}$$

$$\textit{fitness}_{11} = \frac{1}{N}\sum_{n=1}^{N} F_1(f_n) \quad \begin{matrix} 1.92 \le f_n \le 2.17\,\text{GHz} \\ 2.515 \le f_n \le 2.675\,\text{GHz} \end{matrix} \tag{5}$$

$$F_1(f_n) = \begin{cases} 10, |S_{11(n)}| \ge 10 & 1.92 \le f_n \le 2.17\,\text{GHz} \\ |S_{11(n)}|, |S_{11(n)}| \le 10 & 2.515 \le f_n \le 2.675\,\text{GHz} \end{cases} \tag{6}$$

$$\textit{fitness}_{12} = \frac{1}{N}\sum_{n=1}^{N} F_2(f_n) \quad 2.17 \le f_n \le 2.515\,\text{GHz} \tag{7}$$

$$F_2(f_n) = \begin{cases} 10, |S_{11(n)}| \le 10 \\ S_{11(n)} + 20, |S_{11(n)}| \ge 10 \end{cases} \quad 2.17 \le f_n \le 2.515\,\text{GHz} \tag{8}$$

N in the above equation is defined as the population size.

The radiation efficiency of the microstrip antenna is selected as optimization objective 2, and the objective function is defined as follows:

$$\begin{aligned} \textit{fitness 2} \;=\; & 0.5\,\text{Radiation efficiency}\,(f_{2.05\,\text{GHz}}) \\ & +0.5\,\text{Radiation efficiency}\,(f_{2.6\,\text{GHz}}) \end{aligned} \tag{9}$$

Considering the accuracy requirements of multi-frequency antennas, *fitness 1* should be as close to 10 as possible. The radiation efficiency of the antenna is typically greater than 0.5, and a value approaching 1 indicates excellent antenna performance. Therefore, *fitness 2* should be greater than 0.5 and ideally approach 1.

The factors influencing the notch performance are the structural parameters and loading position of the metamaterial. Therefore, j_1, j_2, j_3, j_4, j_5, j_p, and j_g are defined as the optimization parameters, where j_p is the loading position parameter, and the others are structural parameters. The potential values are:

$$X_c = [j_1, j_2, j_3, j_4, j_5, j_p, j_g] = \begin{cases} [15, 4, 2, 2, 2, 10, 0.2]_{\text{min}} \\ [20, 10, 5, 5, 4, 12, 0.6]_{\text{max}} \end{cases}$$

Components of the Genetic Algorithm (GA) [19, 20]: Using binary coding, the population size N is set as 150, and the maximum number of iterations is 20. In the sequential domain patching part, the two optimal solutions generated by the GA are set as boundary points, and the patching is performed according to the patch distance d. After simulation, the approximate Pareto solution set is obtained, yielding the following optimization parameters (unit: mm): $j_1 = 17.032$, $j_2 = 6.875$, $j_3 = 3.111$, $j_4 = 4.298$, $j_5 = 2.438$, $j_p = 11.247$, and $j_g = 0.5$.

Figure 2(c) shows the S-parameter diagram of the dual-band antenna. The simulation of S_{11} parameters and radiation efficiency of the optimized dual-band antenna shows that the antenna operates in two bands: 1.73–2.17 GHz and 2.51–2.79 GHz. Moreover, the radiation efficiency of the two bands is greater than 0.9, and the 5G dual-band antenna with working bands n1 and n41 is realized.

2.3. Four-band Antenna

2.3.1. Asymmetric ELC Metamaterial

Based on the previously developed dual-band antennas, the operating bands of 3.5 GHz and 4.9 GHz are realized by loading asymmetric ELC metamaterials. To reduce the number of metamaterials, the symmetrical ELC structure is replaced by an asymmetric structure, as shown in Fig. 3.

Two surface loading modes of ELC are considered: (1) front side of the dielectric plate, that is, on both sides of the transmission line; and (2) back of the dielectric plate, that is, above the ground. The S-parameter simulation shows that when ELC is loaded onto both sides of the transmission line, the antenna incorporates two additional frequency bands. Therefore, the ELC is loaded onto both sides of the transmission line, as shown in Fig. 3.

TABLE 1. Parameters of initial asymmetric ELC structures.

Variable	a	b	W	d_1	d_2	g_1	g_2	w	ww
Parameter [mm]	3	3	6	0.3	0.1	1.6	1.6	0.2	0.5

TABLE 2. Parameters of the four-band antenna.

Variable	a	b	d_1	d_2	g_1	g_2	w	ww	x	y
Parameter [mm]	3.398	3.276	0.448	0.144	2.199	1.199	0.411	0.993	3.178	0.461

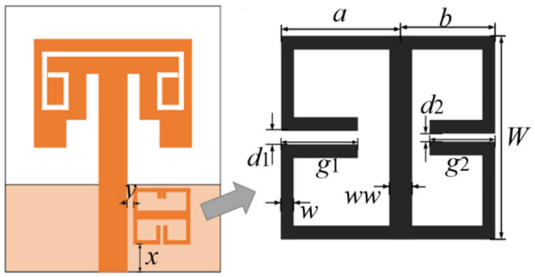

FIGURE 3. Four-band antenna and asymmetric ELC metamaterials.

The resonant frequency of the asymmetric ELC structure is calculated using Equation (10):

$$f = \frac{1}{2\pi\sqrt{2L_eC}} \tag{10}$$

where C is the equivalent capacitance of a parallel plate capacitor formed by g_1 and g_2, and L_e is the equivalent inductance of the ring.

The equivalent capacitance C is calculated using Equation (11):

$$C = \frac{2\varepsilon_0\varepsilon_r g_1 t}{d_1} + \frac{2\varepsilon_0\varepsilon_r g_2 t}{d_2} \tag{11}$$

where ε_0 is the dielectric constant in vacuum, ε_r the relative dielectric constant, and t the thickness of the copper layer.

The equivalent inductance L_e is calculated using Equation (12):

$$L_e = \frac{\mu_0}{2\pi}\left[\ln\left(\frac{2l}{w+t}\right) - 0.2235\ln\left(\frac{w+t}{l}\right) + 0.5\right] \tag{12}$$

where l is the total length of the loop, w the line width, t the thickness of the metal layer, and μ_0 the permeability in vacuum.

The ELC metamaterial structure is simulated and optimized using the parameter scanning method. The determined parameters are listed in Table 1. The S-parameter simulation of the metamaterial shows that two different resonant points are generated at 3.41 GHz and 4.67 GHz. The ELC parameters are substituted into Equations (10)–(12) [18], and two resonant frequency values of 3.40 GHz and 4.74 GHz are obtained, which are consistent with the simulation values and initially satisfy the design requirements.

W is set to the width of the ELC structure, and we set it to 6 mm as no variable. Parameter scanning reveals that the side lengths a and b of the asymmetric ELC structure, lengths g_1 and g_2 of parallel plates, distances d_1 and d_2 of parallel plates, line width w of the loop line, and line width ww of the center line influence the resonance point. Therefore, these variables are the variables optimized by the algorithm.

2.3.2. MSDP Algorithm

Through the co-simulation of HFSS and MATLAB software, the asymmetric ELC structure parameters and loading position are considered optimization variables, and the multi-objective optimization of the antenna is conducted using the MSDP algorithm. The S_{11} and radiation efficiency of the antenna are selected as optimization targets, as indicated in Equations (4)–(9). Only the working frequency band of the objective function needs to be changed, and the settings are defined before algorithm optimization. The two resonant points of the asymmetric ELC metamaterial are selected at 3.5 GHz and 4.9 GHz, and the value range of the optimization variables is determined according to the initial structural parameters presented in Table 1.

$$\begin{aligned} X_c &= [a, b, d_1, d_2, g_1, g_2, w, ww, x, y] \\ &= \begin{cases} [2, 2, 0.1, 0, 1, 1, 0.1, 0.1, 1, 0.2]_{\min} \\ [5, 5, 0.5, 1, 3, 3, 0.5, 1, 5, 0.8]_{\max} \end{cases} \end{aligned}$$

In the above equation, a, b, d_1,d_2, g_1, g_2, w, and ww are structural parameters; and x and y are loading position parameters.

GA algorithm part: The population number is set as 200, and the maximum number of iterations is 15. The sequential domain patching method is then used to complete the following operations. After simulation, the approximate Pareto solution set is obtained, and the optimized antenna parameters are outlined in Table 2 (unit: mm).

3. SIMULATION

3.1. Antenna Operating Band

Figure 4 shows the simulation results of the S_{11} parameters of the optimized antenna, revealing four operating frequency bands. The metamaterial is etched on the radiation

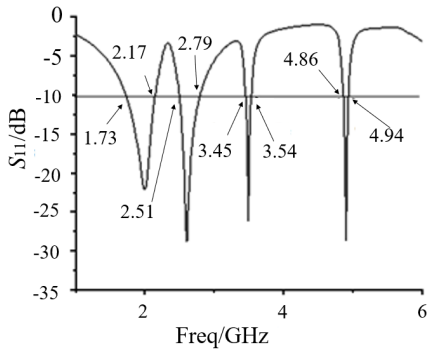

FIGURE 4. S_{11} parameter of four-band antenna.

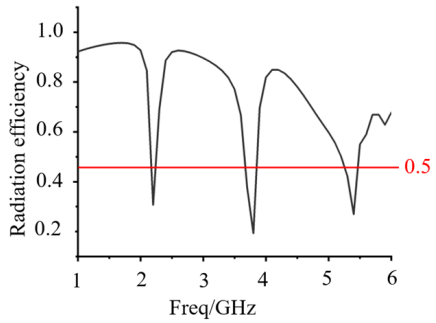

FIGURE 5. Radiation efficiency of four-band antenna.

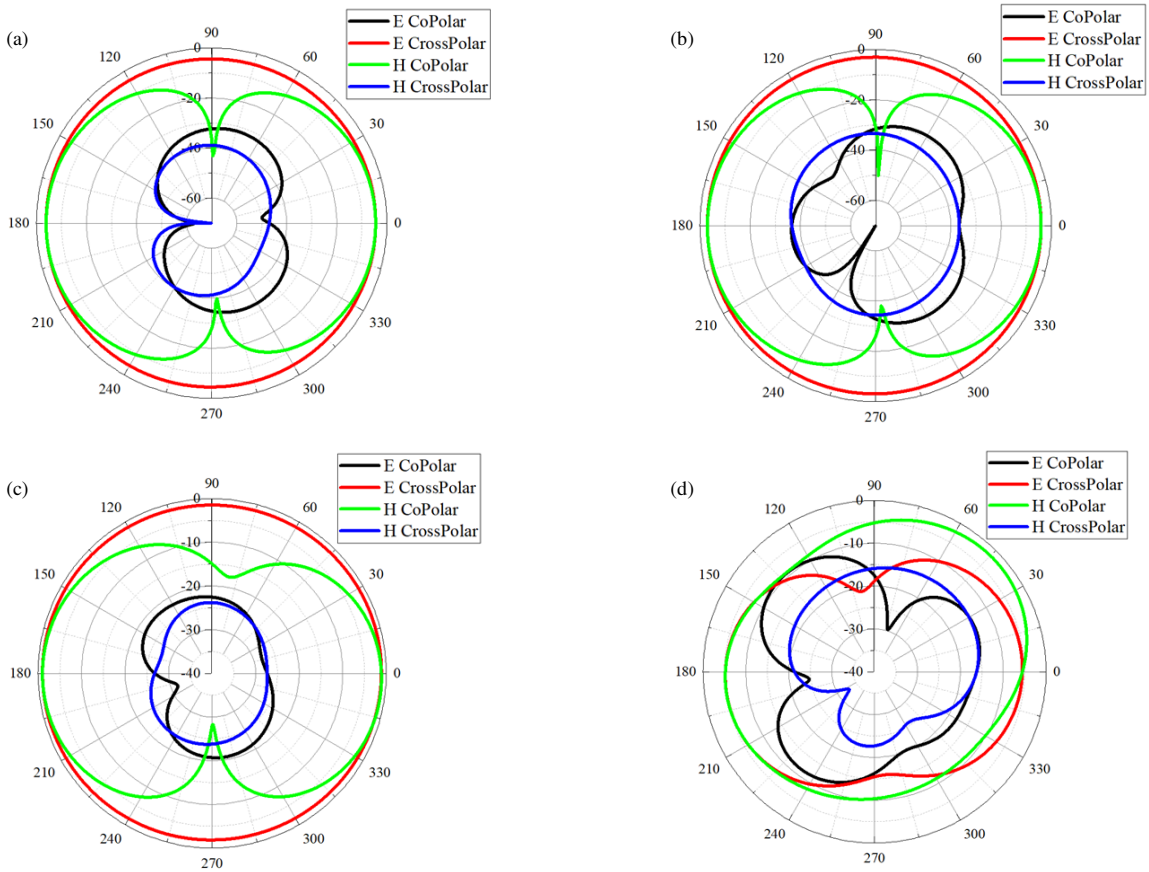

FIGURE 6. Radiation pattern of multi-frequency antenna. (a) 1.95 GHz. (b) 2.65 GHz. (c) 3.5 GHz. (d) 4.9 GHz.

patch of the original antenna to achieve operating bands of 1.73–2.17 GHz and 2.51–2.79 GHz. Two high-frequency bands (3.45–3.54 GHz and 4.86–4.94 GHz) are generated by loading asymmetric ELC metamaterials. By etching the metamaterial on the radiation patch and loading the metamaterial on the transmission line side, four-band antennas with operating frequency bands n1, n41, 3.5G, and 4.9G are realized.

3.2. Radiation Efficiency

The radiation efficiency of the four-band antenna is shown in Fig. 5. The radiation efficiency of the four working bands of the antenna is greater than 0.5, which meets the design requirements.

3.3. Radiation Patterns

Figure 6 shows the direction diagram of the E and H planes of the multi-frequency antenna at four operating frequency points. The figure also shows the co-polarized and cross-polarized patterns of each plane. The antenna exhibits satisfactory low-frequency omnidirectional radiation. Although the high-frequency pattern is slightly degraded, it is still considered to be approximately omnidirectional.

3.4. Analysis of Metamaterial Loading Mechanism

3.4.1. Surface Current Distribution

Figure 7 shows the surface current distribution at frequencies of 1.95 GHz, 2.65 GHz, 3.5 GHz, and 4.9 GHz. In the cases shown

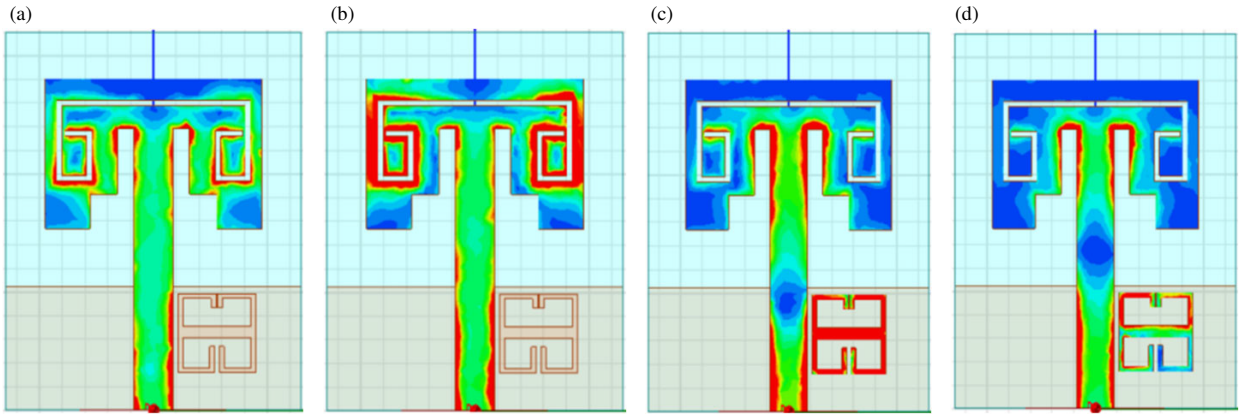

FIGURE 7. Surface current distribution. (a) 1.95 GHz. (b) 2.65 GHz. (c) 3.5 GHz. (d) 4.9 GHz.

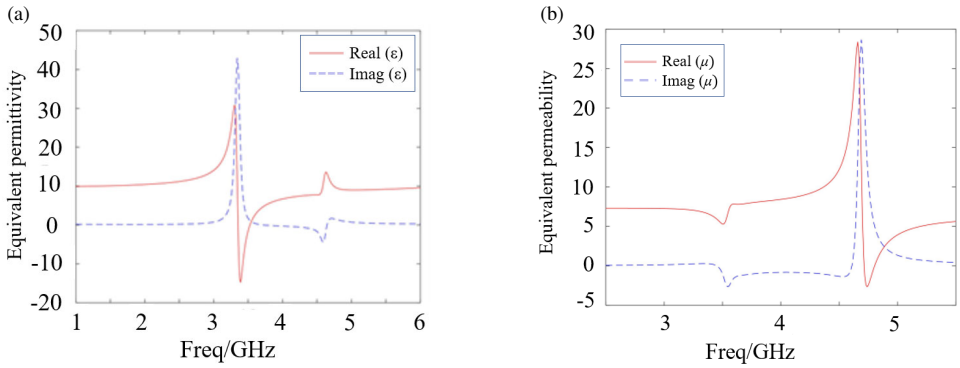

FIGURE 8. (a) Equivalent permittivity. (b) Equivalent permeability.

in Figs. 7(a) and (b), the current is mainly concentrated on the radiation patch, indicating that n1 and n41 are generated by the patch. The currents of the antennas shown in Figs. 7(c) and (d) are mainly concentrated on the asymmetric ELC metamaterial, indicating that 3.5G and 4.9G are generated by metamaterial resonance. These results show that the current distribution on the surface can be altered by etching the spiral metamaterial and loading the asymmetric ELC metamaterial.

3.4.2. Analysis of Metamaterial Properties

The equivalent permeability and permittivity of the helical and ELC resonant elements are determined using the S-parameter inversion method [21]. The helical resonant ring is a single negative permeability metamaterial at 2.31 GHz. The real part value of the equivalent permittivity is 12.61, and the real part value of the equivalent permeability is -22.35.

The calculated ELC metamaterial properties are shown in Fig. 8. At 3.41 GHz, the real part value of the equivalent permittivity is -14.55, and the real part value of the equivalent permeability is 6.34, corresponding to a single negative permittivity metamaterial. At 4.67 GHz, the real part value of the equivalent permittivity is 13.4, and the real part value of the equivalent permeability is -2.6, corresponding to a single negative permeability metamaterial. These metamaterial properties of the asymmetric ELC structure at the resonant point are the underlying reason for its excellent resonant performance, facilitating precise regulation of the resonant band.

4. RESULTS

The multi-frequency antenna is processed using the wet etching method, and the front view of the antenna is shown in Fig. 9(a). The overall size of the antenna is 26 mm $\times$ 32 mm $\times$ 1.6 mm. A vector network analyzer (Agilent N5230A, USA) is used to measure the S-parameter of the actual antenna. Fig. 9(b) shows the test setup.

Figure 10 shows a comparison of the multi-frequency antenna S_{11} parameter test results and simulation results. The antenna operates within two frequency bands in the low-frequency range (1.68–2.17 GHz and 2.55–2.74 GHz), consistent with the simulation results (1.73–2.17 GHz and 2.51–2.79 GHz). The operating frequency band at 3.5G is 3.53–3.59 GHz, which coincides with the simulated frequency band of 3.45–3.54 GHz. The operating frequency band at 4.9G is 5.04–5.12 GHz, which is slightly deviated compared with the simulation band (4.86–4.94 GHz).

Table 3 lists the target frequency bands of the multi-frequency antenna, simulated frequency bands after algorithm optimization, measured operating frequency bands, and rela-

TABLE 3. Bands of multi-frequency antenna.

Target band [GHz]	Optimized post-band [GHz]	Target band [GHz]	Target band [GHz]
1.92–2.17	1.73–2.17	1.68–2.17	7.14%
2.52–2.68	2.51–2.79	2.55–2.74	1.68%
3.45–3.55	3.45–3.54	3.53–3.59	1.69%
4.85–4.95	4.86–4.94	5.04–5.12	3.55%

TABLE 4. Comparison of center frequency errors in this and existing studies.

Ref.	Number of bands	Center frequency at maximum error [GHz]	Maximum error of center frequency [MHz]	Minimum error of center frequency [MHz]	Average error of center frequency [MHz]
[22]	1	4.01	304	74	151.5
[23]	2	4.68	236	80	158
[24]	2	28.54	408	8	194.25
[25]	3	2.30	330	42	149
[26]	3	5.09	87	44	69.25
[27]	4	3.29	124	17	71.75
[28]	4	6.62	234	9	114.5
[29]	4	5.09	149	102	123.5
[30]	6	12.09	2174	60	962.25
This work	4	5.08	110	5	68.5

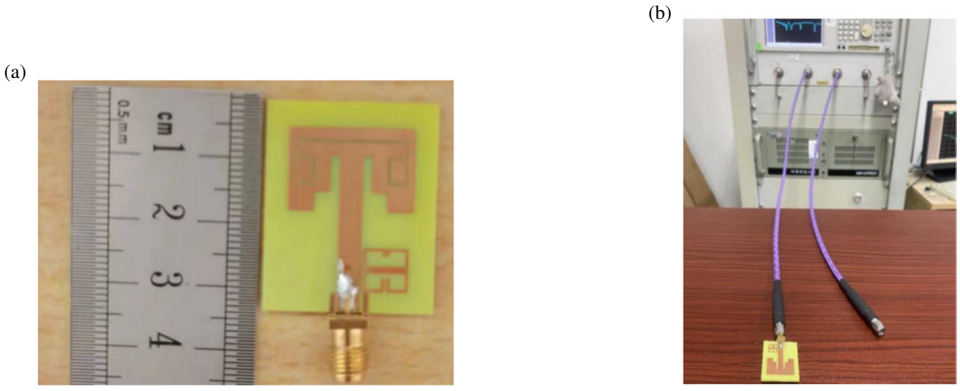

FIGURE 9. (a) Front view of the antenna. (b) Test setup.

tive errors between the measured and target frequency bands. The relative error of the frequency band endpoints represents the upper and lower limit cutoff frequency points. According to Equation (13), the relative error of the frequency band is considered the average value of the relative error of frequency points at both ends. The measured errors of the four groups of the working bands range from as low as 1.68% to as high as 7.2%. The measurement results show that the multi-band antenna can be accurately controlled using the proposed design method.

$$\text{Frequency band relative error} = \frac{|f_{\text{measure}} - f_{\text{target}}|}{f_{\text{target}}} \quad (13)$$

Between the measured and simulated results, a certain deviation is observed, attributable to several factors: (1) In the simulation, the dielectric constant of the FR4 dielectric plate is set to the ideal value of 4.4. However, the dielectric constant of the actual antenna dielectric plate may exhibit a certain deviation. (2) Processing errors may be introduced in the process of printing the PCB and welding the SMA head. (3) Because the test is conducted in a conventional electromagnetic environment, multipath interference of electromagnetic signals may contribute to errors at high frequencies.

The comparison work is completed by calculating the error between the simulation and measured operating center frequency of the antenna, as listed in Table 4. The accuracy

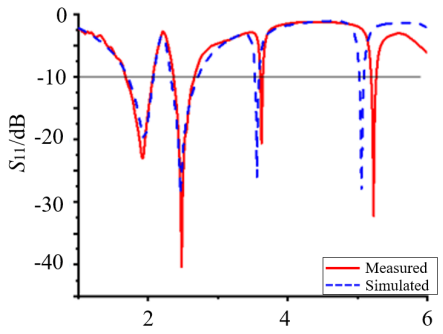

FIGURE 10. Measurement and simulation results for S_{11} parameters.

of antenna band design is comprehensively investigated from three aspects: maximum error, minimum error, and average error. The average measured error of the designed antennas is 68.5 MHz, which is smaller than the ten antennas in the table. The maximum measured error reached 110 MHz, which was only higher than 87 MHz in [26]. The minimum measured error of this antenna is only 5 MHz, which is much lower than other antennas. The antenna in this work operates in four frequency bands. In the design process of multi-band antennas, the design complexity increases with the number of frequency bands. For instance, the average error of the six-band antenna in [30] is 962.25 M. However, compared with other antennas, especially the single-band antenna in [22], the antenna in this work still accurately achieves the target frequency band.

5. CONCLUSIONS

This paper presents a design method for a 5G multi-frequency antenna using the MSDP method. First, a rectangular patch antenna with a frequency band of 1.92–2.72 GHz is improved. A spiral notch metamaterial is etched onto the patch to modify the antenna from a single frequency to a dual-frequency configuration. To reduce the number of resonant units loaded on the transmission line side, the traditional ELC resonator is improved, and the asymmetric ELC resonator is designed to realize the four-band antenna by generating two different resonant points through a single resonant structure. To improve the accuracy and design efficiency of the target working band of the antenna, a multi-objective sequential domain patching method is introduced to optimize the loaded metamaterial structure and loading position, leveraging the S_{11} parameters and radiation efficiency as objective functions. Finally, a four-band antenna with working frequency bands of 1.73–2.17 GHz, 2.51–2.79 GHz, 3.45–3.54 GHz, and 4.86–4.94 GHz is designed, and the error between the measured and observed frequencies is measured.

In general, compared with the traditional antenna design optimization method, optimization of the antenna working band using an intelligent algorithm results in enhanced accuracy. In instances with modified working frequency bands, the proposed design method can effectively improve the design efficiency and working performance of the antenna simply by changing the objective function, facilitating the design of high-performance antennas.

REFERENCES

[1] Yuan, J. D. and X. J. Meng, "Research on the random rolling RFID detection tag antenna on metal surface," *Chinese Journal of Scientific Instrument*, Vol. 11, 115–122, 2021.

[2] Vijetha, T. and D. R. Krishna, "Dual band notch antenna for ultra wide band applications," in *2022 IEEE Microwaves, Antennas, and Propagation Conference (MAPCON)*, 1961–1965, Bangalore, India, 2022.

[3] Kumar, O. P., P. Kumar, and T. Ali, "A novel ultrawideband antenna with band notching facilities at WLAN, C-band, and X-band," in *2022 IEEE 19th India Council International Conference (INDICON)*, 1–6, Kochi, India, 2022.

[4] Rajkumar, R. and K. U. Kiran, "A compact metamaterial multiband antenna for WLAN/WiMAX/ITU band applications," *AEU — International Journal of Electronics and Communications*, Vol. 70, No. 5, 599–604, 2016.

[5] Khajeh Mohammad Lou, R., M. Naser-Moghadasi, and R. A. Sadeghzadeh, "Compact multi-band circularly polarized CPW fed antenna based on metamaterial resonator," *Wireless Personal Communications*, Vol. 94, 2853–2863, 2017.

[6] Wa'il, A. G. A.-T., R. M. Shaaban, and A. P. Duffy, "Design, simulation, and fabrication of a double annular ring microstrip antenna based on gaps with multiband feature," *Engineering Science and Technology, An International Journal*, Vol. 29, 101033, 2022.

[7] Verma, U., M. P. Singh, and S. Ghosh, "Dual band millimeter wave MIMO antenna loaded with SRRs for 5G applications," in *2022 IEEE Wireless Antenna and Microwave Symposium (WAMS)*, 1–3, Rourkela, India, 2022.

[8] Paul, P. M., K. Kandasamy, and M. S. Sharawi, "A tri-band slot antenna loaded with split ring resonators," *Microwave and Optical Technology Letters*, Vol. 59, No. 10, 2638–2643, 2017.

[9] Xu, Q., H. C. Zhou, and Y. W. Hu, "Windmill multi-frequency antenna with split ring resonator," *Chinese Journal of Electron Devices*, Vol. 42, No. 3, 557–562, 2019.

[10] Tian, Y. S. and L. P. Han, "A compact dual-band slot antenna loaded with metamaterial unit cell," *Journal of Shanxi University (Nat. Sci. Ed.)*, Vol. 45, No. 2, 393–399, 2022.

[11] Wang, W. and Y. Zhou, "Energy harvesting surfaces in complex electromagnetic environments," *Electric Measurement Technology*, Vol. 40, No. 9, 6–9, 2017.

[12] Huang, Z. M., "Improved flamingo search algorithm and its application in antenna optimal design," Ph.D. dissertation, Donghua University, Shanghai, China, 2023.

[13] Nan, J., W. Sun, Y. Du, and M. Wang, "One-dimensional convolutional neural network modeling method for ultra-wideband antenna," *Journal of Electronic Measurement and Instrumentation*, Vol. 37, No. 2, 204–210, 2023.

[14] Dong, Y. Z., J. H. Zhou, and Y. G. Wang, "Topology optimization of high-gain metamaterial microstrip antenna based on bagua elements," *Journal of Microwaves*, Vol. 37, No. 5, 16–22, 2021.

[15] Nan, J. C., X. Y. Cao, and M. M. Gao, "A research method for reverse modeling of ultra-wideband antenna with dual notch," in *Proceedings of the 2021 National Microwave and Millimeter Wave Conference*, Vol. 1, 382–384, China Academic Journal Electronic Publishing House, Beijing, 2021.

[16] Liu, Y., "A multi-objective optimization method for microwave devices," Ph.D. dissertation, Harbin Institute of Technology, Harbin, Heilongjiang, China, 2019.

[17] Singh, G. and U. Singh, "Triple band-notched UWB antenna design using a novel hybrid optimization technique based on DE

and NMR algorithms," *Expert Systems with Applications*, Vol. 184, 115299, 2021.

[18] Chen, J. Y., "Application of metamaterial loading technology in antenna design," Ph.D. dissertation, Dalian Jiaotong University, Dalian, China, 2023.

[19] Rahmat-Samii, Y., "Genetic algorithm (GA) and particle swarm optimization (PSO) in engineering electromagnetics," in *17th International Conference on Applied Electromagnetics and Communications, 2003, ICECom 2003*, 1–5, Dubrovnik, Croatia, 2003.

[20] Zhang, X. and Z. Xue, "Optimized design of multi-beam antenna based on real-coded genetic algorithm," *Journal of Microwaves*, Vol. 34, No. 6, 58–61, 2018.

[21] Deng, B., T. Tang, and Y. She, "Design of active frequency selective surface based on square single opening ring metamaterials," *Journal of Chengdu University of Information Techonology*, Vol. 33, No. 1, 39–43, 2018.

[22] Wang, S., H.-C. Li, Y. Li, Z.-C. Guo, G. Zhang, L. Yang, and R. Gómez-García, "A wideband end-fire stepped slot antenna with gain enhancement and filtering capability," *IET Microwaves, Antennas & Propagation*, Vol. 18, No. 6, 422–429, 2024.

[23] Kimura, Y., S. Saito, Y. Kimura, and M. Tatematsu, "Design and measurement of a linearly dual-polarized dual-band and wideband multi-ring microstrip antenna fed by two l-probes," in *2020 International Symposium on Antennas and Propagation (ISAP)*, 789–790, Osaka, Japan, 2021.

[24] Alamdar, S., S. Bagherkhani, F. D. Flaviis, and S. Saadat, "Millimeter wave dual-band antenna array on a thin flexible substrate for 5G applications," in *2024 United States National Committee of URSI National Radio Science Meeting (USNC-URSI NRSM)*, 61–62, 2024.

[25] Iswandi, M. N. Z. Akbar, A. K. D. Jaya, and E. S. Rahayu, "Modification of multi band printed dipole antenna for indoor base station of LTE systems," in *2018 10th International Conference on Information Technology and Electrical Engineering (ICITEE)*, 551–555, Bali, Indonesia, 2018.

[26] Xie, Y., F.-C. Chen, and J.-F. Qian, "Design of integrated duplexing and multi-band filtering slot antennas," *IEEE Access*, Vol. 8, 126 119–126 126, 2020.

[27] Liu, S., S.-S. Qi, W. Wu, and D.-G. Fang, "Single-layer single-patch four-band asymmetrical U-slot patch antenna," *IEEE Transactions on Antennas and Propagation*, Vol. 62, No. 9, 4895–4899, 2014.

[28] Neeththi Aadithiya, B., S. Vijyahlakshmi, K. S. Shineka, and M. Vandhana, "Compact octagonal quad-band antenna for UWB applications," in *2023 International Conference on Innovative Data Communication Technologies and Application (ICIDCA)*, 989–992, Uttarakhand, India, 2023.

[29] Chen, Q. and Y. Sun, "A miniaturized double-sided UWB-MIMO antenna with four-notched band," in *2022 IEEE 10th Asia-Pacific Conference on Antennas and Propagation (APCAP)*, 1–2, Xiamen, China, 2022.

[30] Thaher, R. H., "Circular patch antenna design and analysis for L, S, C, Ku, K, Ka bands, and 5G, wireless applications," in *2022 International Symposium on Multidisciplinary Studies and Innovative Technologies (ISMSIT)*, 1061–1063, Ankara, Turkey, 2022.